AN EFFICIENT LOCALIZED MODEL ORDER REDUCTION FRAMEWORK FOR THE SHAPE OPTIMIZATION OF ADDITIVELY MANUFACTURED LATTICE STRUCTURES ECCOMAS CONGRESS 2024

Philipp Diercks[1], Karen Veroy[2], Annika Robens-Radermacher[1] and Jörg F. Unger[1]

[1] Bundesanstalt für Materialforschung und -prüfung, Unter den Eichen 87, 12205 Berlin, {philipp.diercks, annika.robens-radermacher, joerg.unger}@bam.de, `www.bam.de`

[2] Centre for Analysis, Scientific Computing and Applications (CASA), Department of Mathematics and Computer Science, TU Eindhoven, P.O. Box 513, 5600 MB Eindhoven, The Netherlands, k.p.veroy@tue.nl

Key words: Multiscale methods, Domain decomposition methods, Model order reduction, parameterized PDEs, Shape optimization

Summary. [pd 1]: TODO: add abstract.

1 INTRODUCTION

Additive manufacturing (AM), commonly known as 3D printing, is a manufacturing technique that allows for the production of a wide range of structures and complex geometries. The objects are build successively by adding material layer by layer from three-dimensional models. The technology offers numerous advantages over conventional manufacturing, including greater design flexibility, reduced material waste, and the possibility to produce complex structures with tailored material properties. It has been used in a wide range of applications, including aerospace, biomechanical, automotive, and construction industries [1, 2].

A common engineering practice is to optimize the geometry of a structure by an iterative process, in which an objective function is minimized by systematically choosing parameter values $\boldsymbol{\mu}$ (design variables) and computing the value of the function. In structural mechanics, a prominent example of an objective function is mass or compliance which is a function of the parameter-dependent displacement field $\boldsymbol{u}(\boldsymbol{\mu})$. In each iteration of the optimization process, the geometry is manually changed in the CAD model and the high fidelity finite element (FE) model, also called full order model (FOM), is simply re-evaluated. While this approach is not only an ineffective use of resources, it is also infeasible when solving the FE model is a computationally demanding task, e.g. in multiscale or large-scale industrial applications. Due to the prohibitive cost of even a single FOM solution, the iterative design process cannot be performed using direct numerical simulations. Therefore, we propose a framework based on localized, also called component-based (CB), parametric model order reduction (pMOR). The main idea is to precompute, in a localized manner, empirical basis functions which approximate the solution for some part of the domain without the need to solve the global FOM even once. The global approximation is obtained by a suitable coupling of the local reduced spaces spanned by the

aforementioned basis functions, in which one naturally relies on domain decomposition (DD) strategies. For a review of concepts in localized model order reduction it is referred to [3]. In particular, regarding lattice structures, this approach allows to take advantage of the repetitiveness of the lattice, such that a computation of the local basis is required only for few components, i. e. unit cells.

The computation of the local basis is an essential task in localized pMOR and is often done using the concept of oversampling [4]. In this approach, the target subdomain Ω_{in}, i. e. that part of the domain for which one would like to construct basis functions, is extended and boundary conditions are prescribed on the boundary of the larger so-called oversampling domain Ω to explore possible solutions. In the literature, this oversampling problem is also expressed in terms of a *transfer operator* $\boldsymbol{T}$ that maps the values on the boundary $\partial\Omega$ to the unknown solution restricted to the target subdomain $\boldsymbol{u}(\boldsymbol{\mu})|_{\Omega_{\mathrm{in}}}$. The construction of (optimal) local approximation spaces then comprises the calculation of the left singular vectors of this transfer operator [5, 6]. The direct calculation via eigenvalue problems is, however, computationally expensive and the range of the transfer operator, and thus the optimal local approximation spaces can be efficiently approximated by random sampling [7]. Here, the authors treat non-parametrized partial differential equations (PDEs) and to the authors knowledge the extension to the parametric setting for linear problems has not been done yet. In [6], the authors propose a spectral greedy algorithm to construct parameter-independent local approximation spaces and Taddei and Patera [8] propose a combination of transfer eigenproblems and proper orthogonal decomposition (POD). For parameterized nonlinear elliptic PDEs Smetana and Taddei [9] present a randomized local training procedure with global enrichment.

The contributions of the present work are given as follows. First, as references [6, 8] do not make use of range approximation via random sampling, a suitable training strategy to construct local approximation spaces for parameterized linear problems via random sampling is discussed. Herein, the approach given in [8], identified as a *distributed approximate POD* (see also [10]), is adopted to range approximation via random sampling. Second, a framework for the shape optimization of lattice structures is proposed. It combines the aforementioned algorithm to construct local approximation spaces with an auxiliary problem, as in [11], to facilitate geometrical parametrizations of the unit cell and the matrix version [12] of the empirical interpolation method (EIM) [13, 14] to ensure online efficiency of the final reduced order model (ROM). Furthermore, the global approximation space is constructed from the local spaces using the partition of unity method or generalized finite element method (GFEM) [15, 16].

The rest of the article is organized as follows. In section 2, the building blocks of the shape optimization framework are described. In particular, the range approximation of a parametric transfer operator is discussed. Section 3 comprises the numerical experiments. Based on the example of a graded concrete slab, the quality of the local spaces generated by the method described in section 2.2.1 is analyzed, the proposed ROM is validated, and results for the solution of a shape optimization problem are presented. Finally, conclusions are given in section 4.

TODO: add note on notation where appropriate.[pd]

2 METHOD

The method proposed in this article is a localized pMOR framework for the shape optimization of lattice structures. First, the auxiliary problem to model geometrical parameterizations

is introduced in section 2.1. Second, the construction of local approximation spaces is described in section 2.2. Herein, the parametric oversampling problem and training strategy to approximate the range of the corresponding parametric transfer operator are discussed. Third, it is outlined how a global approximation is obtained from local approximation spaces via the GFEM. Finally, the necessity and use of hyper-reduction (in the form of empirical interpolation) to ensure an online-efficient ROM is detailed in section 2.4.

2.1 Auxiliary Problem

The approach adopted in this work to facilitate geometrical parameterizations belongs to the class of surface-based deformations [17] and is based on transformations $\Phi_{\boldsymbol{\mu}}$ that map each material point $\boldsymbol{x}_{\mathrm{p}}$ of a parameter-independent reference or parent domain Ω^{p} to a point $\boldsymbol{x}_{\boldsymbol{\mu}}$ in the parameter-dependent current or physical domain $\Omega^{\boldsymbol{\mu}}$. In the context of shape optimization of lattice structures, our objective is to determine the mapping $\Phi_{\boldsymbol{\mu}}$ for a single unit cell, see fig. 1, and use it to describe the change in geometry of each unit cell throughout the structure. An auxiliary problem based on the equations of linear elasticity is solved to obtain such domain transformations, following the approach outlined in [11], and briefly repeated here for completeness.

The transformation map $\Phi_{\boldsymbol{\mu}}$ from parent to physical domain $\Phi_{\boldsymbol{\mu}} : \Omega^{\mathrm{p}} \mapsto \Omega^{\boldsymbol{\mu}}$ is given by $\boldsymbol{x}_{\boldsymbol{\mu}} = \Phi_{\boldsymbol{\mu}}(\boldsymbol{x}_{\mathrm{p}}) = \boldsymbol{x}_{\mathrm{p}} + \boldsymbol{d}(\boldsymbol{x}_{\mathrm{p}}; \boldsymbol{\mu})$, with $\boldsymbol{d}(\boldsymbol{x}_{\mathrm{p}}; \boldsymbol{\mu})$ being the transformation displacement field. The transformation displacement is determined by solving the following linear elastostatic auxiliary problem.

$$\boldsymbol{\nabla} \cdot \left(\hat{\mathbb{C}} \cdot \cdot \frac{1}{2} \left(\boldsymbol{d} \otimes \boldsymbol{\nabla} + \boldsymbol{\nabla} \otimes \boldsymbol{d} \right) \right) = \boldsymbol{0} \, , \quad \text{in } \Omega^{\mathrm{p}} \, , \tag{1}$$

$$\boldsymbol{d} = \boldsymbol{0} \, , \quad \text{on } \partial\Omega^{\mathrm{p}} \, , \tag{2}$$

$$\boldsymbol{d} = \boldsymbol{x}_{\mu} - \boldsymbol{x}_{\mathrm{p}} \, , \quad \text{on } \partial\Omega^{\mathrm{p}}_{\mathrm{int}} \, . \tag{3}$$

The stiffness tetrad of the auxiliary problem is defined as

$$\hat{\mathbb{C}} = \hat{\lambda} \boldsymbol{I} \otimes \boldsymbol{I} + 2\hat{\mu}\mathbb{I} \, , \quad \text{with} \quad \hat{\lambda} = \frac{\nu}{(1+\nu)(1-2\nu)} \quad \text{and} \quad \hat{\mu} = \frac{1}{2(1+\nu)} \, . \tag{4}$$

With $\boldsymbol{x}_{\boldsymbol{\mu}}$ known for all points on the parent interface $\partial\Omega^{\mathrm{p}}_{\mathrm{int}}$, the desired transformation (e.g. enlarging/shrinking of the voids radius) is enforced by prescribing eqs. (2) and (3).

Given the transformation displacement $\boldsymbol{d}(\boldsymbol{x}_{\mathrm{p}}; \boldsymbol{\mu})$, the variational formulation is formulated over the parameter-independent parent domain Ω^{p} instead of the parameter-dependent physical domain $\Omega^{\boldsymbol{\mu}}$. This introduces the parameter dependence in the variational formulation as shown in the following subsections, but has the advantage that numerical integration can be carried out over the fixed parent domain and thus no re-meshing is required. However, for each new parameter value $\boldsymbol{\mu}$ for which the model is to be evaluated, we first need to solve the auxiliary problem. Nevertheless, this does not pose a problem, since the solution of the auxiliary problem is well amenable to acceleration via established MOR techniques and it is referred to [11] for further details.
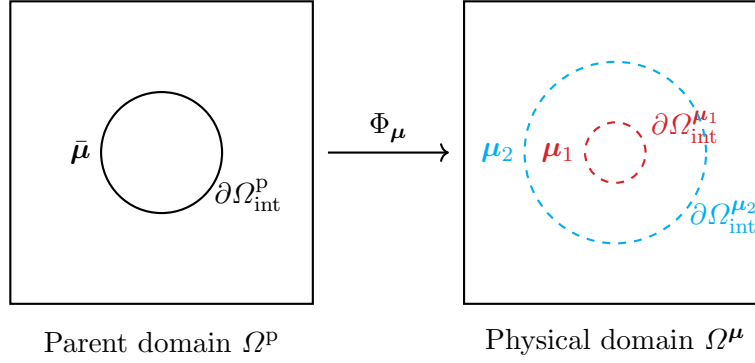
Figure 1: Transformation map $\Phi_{\boldsymbol{\mu}}$ from parent to physical domain on the example of the unit square domain with a circular void placed in the center. The parameter $\boldsymbol{\mu}$ controls the radius of the void.

2.2 Construction of local approximation spaces

In this paper, local approximation spaces are constructed by solving an oversampling problem many times for different parameter values $\boldsymbol{\mu}$ and different (random) boundary conditions. It is therefore useful to cast this oversampling problem in the form of a parameter-dependent transfer operator $\boldsymbol{T_{\mu}}$ that maps the boundary function $\boldsymbol{g}$ to the solution $\boldsymbol{u}(\boldsymbol{\mu})$ in the target subdomain $\Omega_{\text{in}}^{\boldsymbol{\mu}}$. The approximation of the range of this transfer operator is then the sought after local approximation space, see [7].

First, the global domain $\Omega_{\text{gl}}^{\boldsymbol{\mu}}$ and a non-overlapping domain decomposition

$$\Omega_{\text{gl}}^{\boldsymbol{\mu}} = \cup_{i=1}^{N_{\text{cells}}} \Omega_i^{\boldsymbol{\mu}} \tag{5}$$

is introduced. In the context of lattice structures, each subdomain $\Omega_i^{\boldsymbol{\mu}}$ corresponds to a unit cell. Next, a coarse grid partition of the global domain and a fine grid partition of the unit cell is introduced as shown in fig. 2. Figure 2 also shows one exemplary oversampling domain $\Omega^{\boldsymbol{\mu}}$. The oversampling problem (given for linear elastostatics) then comprises the solution of the following boundary value problem.

$$\begin{aligned}
-\boldsymbol{\nabla} \cdot \boldsymbol{\sigma}(\boldsymbol{u}(\boldsymbol{\mu})) &= \boldsymbol{0} &&\text{in } \Omega^{\boldsymbol{\mu}} \subset \Omega_{\text{gl}}^{\boldsymbol{\mu}}, \\
\boldsymbol{\sigma}(\boldsymbol{u}(\boldsymbol{\mu})) \cdot \boldsymbol{n} &= \boldsymbol{0} &&\text{on } \Gamma_{\text{N}}^{\boldsymbol{\mu}} := \partial\Omega^{\boldsymbol{\mu}} \cap \Sigma_{\text{N}}^{\boldsymbol{\mu}}, \\
\boldsymbol{u}(\boldsymbol{\mu}) &= \boldsymbol{0} &&\text{on } \Gamma_{\text{D}}^{\boldsymbol{\mu}} := \partial\Omega^{\boldsymbol{\mu}} \cap \Sigma_{\text{D}}^{\boldsymbol{\mu}}, \\
\boldsymbol{u}(\boldsymbol{\mu}) &= \boldsymbol{g} &&\text{on } \Gamma_{\text{out}}^{\boldsymbol{\mu}} := \partial\Omega^{\boldsymbol{\mu}} \setminus \partial\Omega_{\text{gl}}^{\boldsymbol{\mu}}.
\end{aligned} \tag{6}$$

Here, $\boldsymbol{\sigma}$ is the Cauchy stress, $\boldsymbol{n}$ the normal vector and $\boldsymbol{g}$ Dirichlet boundary data to be prescribed on the boundary $\Gamma_{\text{out}}^{\boldsymbol{\mu}}$. The boundaries $\Gamma_{\text{N}}^{\boldsymbol{\mu}}$ and $\Gamma_{\text{D}}^{\boldsymbol{\mu}}$ denote the part of the boundary of the oversampling domain that coincides with the global Neumann boundary $\Sigma_{\text{N}}^{\boldsymbol{\mu}}$ or Dirichlet boundary $\Sigma_{\text{D}}^{\boldsymbol{\mu}}$, respectively. Note that the topology is dependent on the target subdomain $\Omega_{\text{in}}^{\boldsymbol{\mu}}$ and the size of the oversampled region. Considering linear elastic isotropic materials

$$\boldsymbol{\sigma}(\boldsymbol{u}(\boldsymbol{\mu})) = \mathbb{C} \cdot\cdot \boldsymbol{\varepsilon}(\boldsymbol{u}(\boldsymbol{\mu})), \tag{7}$$

with the linear strain tensor as

$$\boldsymbol{\varepsilon}(\boldsymbol{w}) := \frac{1}{2} \left(\boldsymbol{w} \otimes \boldsymbol{\nabla} + \boldsymbol{\nabla} \otimes \boldsymbol{w} \right) , \tag{8}$$

and the stiffness tetrad given in component form as

$$C_{ijkl} = \lambda \delta_{ij} \delta_{kl} + \mu \left(\delta_{ik} \delta_{jl} + \delta_{il} \delta_{jk} \right) , \tag{9}$$

the weak form reads

$$\int_{\Omega^{\boldsymbol{\mu}}} \frac{\partial \boldsymbol{\delta u}}{\partial \boldsymbol{x^{\mu}}} \cdot\cdot \mathbb{C} \cdot\cdot \frac{\partial \boldsymbol{u(\mu)}}{\partial \boldsymbol{x^{\mu}}} \, \mathrm{d}\boldsymbol{x^{\mu}} = \boldsymbol{0} . \tag{10}$$

Herein, $\boldsymbol{\delta u}$ denotes the test function. The weak form is implicitly dependent on the parameter $\boldsymbol{\mu}$ due to the integration carried out over the physical domain $\Omega^{\boldsymbol{\mu}}$. By introducing the deformation gradient of the geometrical transformation[1] as introduced in section 2.1

$$\boldsymbol{F_{\mu}} := \frac{\mathrm{d}\boldsymbol{x^{\mu}}}{\mathrm{d}\boldsymbol{x}^{\mathrm{p}}} \quad \text{and} \quad \mathrm{d}\boldsymbol{x^{\mu}} = \det(\boldsymbol{F_{\mu}}) \, \mathrm{d}\boldsymbol{x}^{\mathrm{p}} , \tag{11}$$

the integration can be carried out over the fixed parent domain

$$\int_{\Omega^{\mathrm{p}}} \left(\frac{\partial \boldsymbol{\delta u}}{\partial \boldsymbol{x}^{\mathrm{p}}} \cdot \boldsymbol{F_{\mu}}^{-1} \right) \cdot\cdot \mathbb{C} \cdot\cdot \left(\frac{\partial \boldsymbol{u(\mu)}}{\partial \boldsymbol{x}^{\mathrm{p}}} \cdot \boldsymbol{F_{\mu}}^{-1} \right) \det(\boldsymbol{F_{\mu}}) \, \mathrm{d}\boldsymbol{x}^{\mathrm{p}} = \boldsymbol{0} . \tag{12}$$

The resolution of eq. (12) and subsequent restriction of the solution to the target subdomain, denoted as $\boldsymbol{u(\mu)}\big|_{\Omega_{\mathrm{in}}^{\mathrm{p}}}$, comprises the solution of the oversampling problem. The transfer operator $\boldsymbol{T_{\mu}} : \mathcal{S} \to \mathcal{R}$, maps for a given parameter value $\boldsymbol{\mu}$ the boundary data $\boldsymbol{g}$ to the solution on the target subdomain $\boldsymbol{u(\mu)}\big|_{\Omega_{\mathrm{in}}^{\mathrm{p}}} = \boldsymbol{T_{\mu}(g)}$. Here, $\mathcal{S}$ and $\mathcal{R}$ are appropriate source and range spaces, respectively. Throughout the paper, we assume a suitable discretization and numerical solution of eq. (12) using the FE method. For details concerning the discretization of the transfer operator (for a fixed parameter value) it is referred to [7].

Finally, we note that the images of $\boldsymbol{T_{\mu}}$ are computed, such that they do not contain any translations or rotations (rigid body modes are removed via orthogonal projection), i. e. they comprise purely *deformational* modes. Moreover, (global) NEUMANN or DIRICHLET boundary conditions prescribed on $\Sigma_{\mathrm{N}}^{\boldsymbol{\mu}}$ or $\Sigma_{\mathrm{D}}^{\boldsymbol{\mu}}$, respectively, have not been considered yet. Therefore, for example, an additional NEUMANN problem[2] has to be solved to enrich the local spaces.

$$\begin{aligned} -\boldsymbol{\nabla} \cdot \boldsymbol{\sigma}(\boldsymbol{u(\mu)}) &= \boldsymbol{0} &&\text{in } \Omega^{\boldsymbol{\mu}} \subset \Omega_{\mathrm{gl}}^{\boldsymbol{\mu}} , \\ \boldsymbol{\sigma}(\boldsymbol{u(\mu)}) \cdot \boldsymbol{n} &= \hat{\boldsymbol{t}} &&\text{on } \Gamma_{\mathrm{N}}^{\boldsymbol{\mu}} := \partial\Omega^{\boldsymbol{\mu}} \cap \Sigma_{\mathrm{N}}^{\boldsymbol{\mu}} , \\ \boldsymbol{u(\mu)} &= \boldsymbol{0} &&\text{on } \Gamma_{\mathrm{D}}^{\boldsymbol{\mu}} := \partial\Omega^{\boldsymbol{\mu}} \cap \Sigma_{\mathrm{D}}^{\boldsymbol{\mu}} , \\ \boldsymbol{u(\mu)} &= \boldsymbol{0} &&\text{on } \Gamma_{\mathrm{out}}^{\boldsymbol{\mu}} := \partial\Omega^{\boldsymbol{\mu}} \setminus \partial\Omega_{\mathrm{gl}}^{\boldsymbol{\mu}} . \end{aligned} \tag{13}$$

Equation (13) is solved on the parent domain employing the pull back as above. Also, for construction of a sufficiently rich local basis it has to be solved for many parameter values $\boldsymbol{\mu}$, but a sampling of the boundary values on $\Gamma_{\mathrm{out}}^{\boldsymbol{\mu}}$ is not required.

---

[1]We note here that the auxiliary problem described in section 2.1 needs to be extended to the oversampling domain, which consists of a union of unit cells. This is straightforward in the current setup, but has the limitation that eq. (2) needs to be satisfied for each unit cell, i. e. the interfaces between them.

[2]The case of inhomogeneous DIRICHLET boundary conditions is analogous.
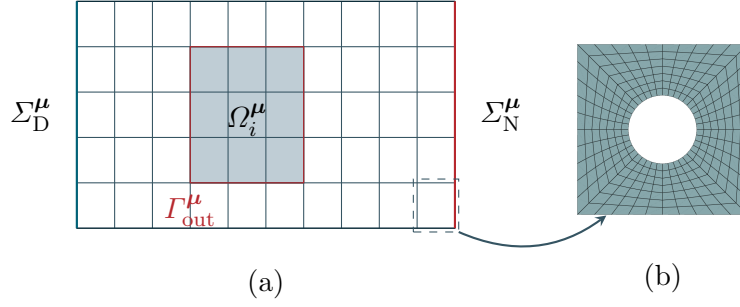
Figure 2: Exemplary coarse grid discretization of the global domain $\Omega_{\text{gl}}^{\boldsymbol{\mu}}$, with target subdomain $\Omega_i^{\boldsymbol{\mu}}$ within oversampling domain $\Omega^{\boldsymbol{\mu}}$ in grey (a) and fine grid discretization of the unit cell (b).

2.2.1 Randomized range finder and proper orthogonal decomposition

Assuming a proper FE discretization of $\boldsymbol{T_\mu}$, next the algorithm to approximate the range of $\boldsymbol{T_\mu}$ for any $\boldsymbol{\mu}$ is discussed. Herein, a strategy for the exploration of the parameter space and sampling of the random boundary conditions in the oversampling are the key challenges. In the present work, the strategy by Taddei & Patera [8] is adopted in which based on the connection between the POD of images of the transfer operator (for certain boundary conditions) and the singular values of the transfer operator they devise a training strategy which is recognized as a distributed approximate POD (see [10]). For each $\boldsymbol{\mu}_j$ in a predefined training set, they compute the singular values of $\boldsymbol{T_{\mu_j}}$ by resolution of an eigenvalue problem and subsequently compute the POD over the set of all eigenvectors. As the authors state, the resolution of the eigenvalue problems may be prohibitive in some cases, and therefore we employ range approximation by random sampling instead.

The procedure for the computation of parameter-independent deformational modes is summarized in algorithm 1. First, an empty snapshot set $\boldsymbol{S}$ and a training set $\boldsymbol{S}_{\text{train}}$ are initialized. The training set $\boldsymbol{S}_{\text{train}}$ has to be sufficiently rich, such that it is a good representation of the parameter space. [**pd** 2]: TODO: add reference to Haasdonk (standard sampling)? Next, for each parameter value $\boldsymbol{\mu}_j \in \boldsymbol{S}_{\text{train}}$ the range of $\boldsymbol{T_{\mu_j}}$ which is now fixed with respect to the parameter value is approximated using Algorithm 1 ADAPTIVERANDOMIZEDRANGEAPPROXIMATION from [7] and the set of snapshots is extended by Gram Schmidt orthogonalization (line 5 & 6). Note that the parameter value $\boldsymbol{\mu}$ and boundary conditions $\boldsymbol{g}$ are not varied at the same time. Finally, the POD is computed over the snapshot set $\boldsymbol{S}$ which yields the parameter-independent space X^n. The dimension of the local space X^n, i.e. the number of local basis functions is denoted by n.

In case of inhomogeneous NEUMANN boundary conditions, after termination of algorithm 1, the NEUMANN problem eq. (13) is solved for each $\boldsymbol{\mu}_j \in \boldsymbol{S}_{\text{train}}$ as well. Following compression via POD the space X^n is enriched by the additional NEUMANN modes.

[**pd** 3]: TODO: explain tolerances to control approximation quality. Refer to HAPOD paper and mention that ε^* can be used to compute tolerances at each node of the tree. [**pd** 4]: TODO: define notation for POD.

Algorithm 1 RRFPOD caption.

1: **function** HAPODRANGEAPPROXIMATION($\boldsymbol{T}$, $\texttt{tol}$, n_t, $\varepsilon_{\text{algofail}}$, N_{train})
   Input: Operator $\boldsymbol{T_\mu}$, target tolerance $\texttt{tol}$, number of testvectors n_t, maximum failure probability $\varepsilon_{\text{algofail}}$, number of parameter samples N_{train}
   Output: space X^n
2:   $\boldsymbol{S} \leftarrow \emptyset$ ▷ initialize snapshot set
3:   $\boldsymbol{S}_{\text{train}} \leftarrow \{\boldsymbol{\mu}_1, \ldots, \boldsymbol{\mu}_{N_{\text{train}}}\}$ ▷ initialize training set
4:   **for** $\boldsymbol{\mu}_j$ in $\boldsymbol{S}_{\text{train}}$ **do**
5:     $\boldsymbol{R} \leftarrow$ ADAPTIVERANDOMIZEDRANGEAPPROXIMATION($\boldsymbol{T_{\mu_j}}$, $\texttt{tol}$, n_t, $\varepsilon_{\text{algofail}}$)
6:     $\boldsymbol{S} \leftarrow$ orthonormalize$(\boldsymbol{S} \cup \boldsymbol{R})$
7:   **end for**
8:   $\boldsymbol{B} \leftarrow \text{POD}(\boldsymbol{S})$
9:   **return** $X^n = \text{span}(\boldsymbol{B})$
10: **end function**

2.3 Construction of a global approximation

Given local approximation spaces X_i^n for each target subdomain Ω_i^{p}, the construction of a global approximation via the GFEM is discussed. The difficulty is that the basis functions of the local spaces X_i^n and X_j^n of two neighboring subdomains Ω_i^{p} and Ω_j^{p} are not conforming on the shared interface $\Gamma_{ij}^{\text{p}} = \partial\Omega_i^{\text{p}} \cap \partial\Omega_j^{\text{p}}$. However, given a suitably[3] defined partition of unity $\{\varphi_i\}$ the local basis functions can be included in the global FE space by multiplication with the standard FE shape functions φ_i, such that a conforming approximation is obtained. The global GFEM space is defined as

$$X_{\text{GFEM}} := \sum_i \varphi_i X_i^n = \left\{ \sum_i \varphi_i \boldsymbol{\xi}_i \mid \boldsymbol{\xi}_i \in X_i^n \right\}. \tag{14}$$

[**pd** 5]: TODO: add figure. This explains best what is going on. [**pd** 6]: TODO: equation for partition of unity and final gfem space. Not sure if I can write this like Babuska.

2.4 Online efficiency

With the global GFEM space, each coarse grid cell (i.e. unit cell of the lattice) can be viewed as a high order FE. For example, it is just a quadrilateral cell with special ansatz functions

- explain approach based on *super elements*: each unit cell is just a quadrilateral cell with special ansatz functions

- challenge: would still need to assemble K of unit cell for each new parameter

- therefore, employ EIM to speed up assembly of K (reduced integration)

3 NUMERICAL EXPERIMENTS

- general stuff like FE cell type and degree

---

[3]According to Definition 1 of [15].

- software: dolfinx version 0.8.0

- PC hardware?

3.1 Graded concrete slab

- introduce graded concrete / problem (gradientenbeton eu); why this is interesting

- sketch of the mechanical problem

- setup regarding the new method?

3.2 Projection error study

3.3 Reduced order model validation

3.4 Shape optimization

4 CONCLUSIONS

REFERENCES

[1] A. du Plessis et al. "Properties and applications of additively manufactured metallic cellular materials: A review". In: *Progress in Materials Science* 125 (Apr. 2022), p. 100918. DOI: 10.1016/j.pmatsci.2021.100918.

[2] P. Wu, J. Wang, and X. Wang. "A critical review of the use of 3-D printing in the construction industry". In: *Automation in Construction* 68 (Aug. 2016), pp. 21–31. DOI: 10.1016/j.autcon.2016.04.005.

[3] A. Buhr et al. "6 Localized model reduction for parameterized problems". In: *Volume 2: Snapshot-Based Methods and Algorithms*. Ed. by P. Benner et al. Berlin, Boston: De Gruyter, 2021, pp. 245–306. DOI: doi:10.1515/9783110671490-006.

[4] T. Y. Hou and X.-H. Wu. "A Multiscale Finite Element Method for Elliptic Problems in Composite Materials and Porous Media". In: *Journal of Computational Physics* 134.1 (June 1997), pp. 169–189. DOI: 10.1006/jcph.1997.5682.

[5] I. Babuska and R. Lipton. "Optimal Local Approximation Spaces for Generalized Finite Element Methods with Application to Multiscale Problems". In: *Multiscale Modeling & Simulation* 9.1 (Jan. 2011), pp. 373–406. DOI: 10.1137/100791051.

[6] K. Smetana and A. T. Patera. "Optimal Local Approximation Spaces for Component-Based Static Condensation Procedures". In: *SIAM J. Sci. Comput.* 38 (5 Jan. 2016). DOI: 10.1137/15m1009603.

[7] A. Buhr and K. Smetana. "Randomized Local Model Order Reduction". In: *SIAM J. Sci. Comput.* 40 (4 Jan. 2018). DOI: 10.1137/17m1138480.

[8] T. Taddei and A. T. Patera. "A Localization Strategy for Data Assimilation; Application to State Estimation and Parameter Estimation". In: *SIAM J. Sci. Comput.* 40 (2 Jan. 2018). DOI: 10.1137/17m1116830.

[9] K. Smetana and T. Taddei. "Localized Model Reduction for Nonlinear Elliptic Partial Differential Equations: Localized Training, Partition of Unity, and Adaptive Enrichment". In: *SIAM J. Sci. Comput.* 45 (3 June 2023). DOI: 10.1137/22m148402x.

[10] C. Himpe, T. Leibner, and S. Rave. "Hierarchical Approximate Proper Orthogonal Decomposition". In: *SIAM J. Sci. Comput.* 40 (5 Jan. 2018). DOI: 10.1137/16m1085413.

[11] T. Guo et al. "Learning constitutive models from microstructural simulations via a non-intrusive reduced basis method: Extension to geometrical parameterizations". In: *Comput. Methods Appl. Mech. Eng.* 401 (Nov. 2022). DOI: 10.1016/j.cma.2022.115636.

[12] F. Negri, A. Manzoni, and D. Amsallem. "Efficient model reduction of parametrized systems by matrix discrete empirical interpolation". In: *Journal of Computational Physics* 303 (Dec. 2015), pp. 431–454. DOI: 10.1016/j.jcp.2015.09.046.

[13] M. Barrault et al. "An 'empirical interpolation' method: application to efficient reduced-basis discretization of partial differential equations". In: *Comptes Rendus. Mathématique* 339.9 (Oct. 2004), pp. 667–672. DOI: 10.1016/j.crma.2004.08.006.

[14] S. Chaturantabut and D. C. Sorensen. "Nonlinear Model Reduction via Discrete Empirical Interpolation". In: *SIAM J. Sci. Comput.* 32 (5 Jan. 2010). DOI: 10.1137/090766498.

[15] I. Babuška and J. M. Melenk. "The partition of unity method". In: *International Journal for Numerical Methods in Engineering* 40.4 (1997), pp. 727–758. DOI: 10.1002/(SICI) 1097-0207(19970228)40:4<727::AID-NME86>3.0.CO;2-N.

[16] I. Babuška, U. Banerjee, and J. E. Osborn. "Generalized Finite Element Methods — Main Ideas, Results and Perspective". In: *International Journal of Computational Methods* 01.01 (June 2004), pp. 67–103. DOI: 10.1142/s0219876204000083.

[17] M. Botsch et al. *Polygon Mesh Processing.* A K Peters/CRC Press, Oct. 2010. DOI: 10.1201/b10688.